Simulated aerodynamic loading of an SH-60B helicopter in a ship's airwake

Christopher H Kääriä[*]
Department of Engineering
University of Liverpool
Liverpool, UK
c.h.kaaria@liv.ac.uk

James S Forrest[*]
Department of Engineering
University of Liverpool
Liverpool, UK
james.forrest@liv.ac.uk

Ieuan Owen[†]
Department of Engineering
University of Liverpool
Liverpool, UK
i.owen@liv.ac.uk

Gareth D Padfield[‡]
Department of Engineering
University of Liverpool
Liverpool, UK
gareth.padfield@liv.ac.uk

This paper describes a simulation study evaluating the aerodynamic loading of a model Sea-Hawk (SH-60B) helicopter in the wake of a simple frigate shape (SFS2). Time-accurate CFD airwakes have been computed using Detached-Eddy Simulation (DES) for two wind-over-deck (WOD) conditions and integrated into the FlightLab simulation environment. A simulated rotorcraft model configured to be representative of an SH-60B has been fixed in space at various locations relative to the flight deck of the ship and immersed in the unsteady airwake for a period of thirty seconds. The forces and moments acting on the helicopter model as a result of the airwake have been recorded and analysed in terms of the helicopter location and WOD condition. The specific time-averaged and unsteady aerodynamic loading characteristics have been identified and analysed in terms of their implications for helicopter handling qualities and potential pilot workload. The underlying causes of the aerodynamic loading characteristics encountered in the simulations have been identified through analysis of the CFD airwake data. The capability of this technique to identify specific loading characteristics and to relate them back to the airwake aerodynamics demonstrates its suitability as a means of comparing the severity of different ship airwakes on helicopter operations. Thus, it is feasible that this method could be used to effectively assess the potential benefits of ship geometry modifications to the ship-helicopter dynamic interface.

Introduction

Landing a maritime helicopter to the flight deck of a ship is a difficult and demanding task for even the most experienced pilots. As well as operating to a restricted landing area and a pitching, rolling and heaving ship, the pilot must also contend with the presence of a highly unsteady flow field over the flight deck. This phenomenon, known as the ship's 'airwake', is caused by the airflow over and around the ship's superstructure as a result of the combined effect of the prevailing wind and the forward motion of the ship.

Over recent years, collaborative international research into the ship-helicopter dynamic interface has investigated flight deck aerodynamics using techniques such as flow visualisation [1-5], wind tunnel anemometry [3-5], and Computational Fluid Dynamics (CFD) [6-8]. As a result, the key features of the airwake are now relatively well understood [9]. Ships are not generally designed with aerodynamics in mind, so the sharp edges of the superstructure lead to unstable flow separation and the formation of vortices, causing large spatial and temporal gradients in the airflow over the flight deck. The degree of unsteadiness in the airwake can be affected by large scale geometric features such as masts, radar domes and weapon systems. The nature and severity of the airwake also varies significantly with wind-over-deck (WOD) speed and direction.

As the pilot moves the helicopter through the airwake during an approach to landing, the highly unsteady airflow causes large fluctuations in the

[*]Postgraduate Research Student [†]Professor of Mechanical Engineering [‡]James Bibby Professor of Aerospace Engineering Presented at the 35th European Rotorcraft Forum, Hamburg, Germany, 21 – 25 September 2009

aerodynamic loading and the rotor response of the helicopter in the closed-loop pilot response frequency range of 0.2-2 Hz [10, 11]. The pilot is then required to take corrective action via the control inputs in order to stabilise aircraft attitude. Consequently, for certain WOD conditions, the pilot workload required to maintain aircraft stability is so high and the pilot's spare capacity to perform ancillary tasks is so reduced, that landing is deemed unsafe for fleet pilots to attempt. Such conditions are then considered outside the safe operational limits of the ship-helicopter combination in question.

The spare control margins available to the pilot throughout an operation are also an important factor to consider in the establishment of safe operational envelopes. If the pilot is required to move a control to within 10% of its maximum travel during a landing task then the capability to respond to large disturbances in that axis is severely compromised. This typically leads to an operational limit being imposed as the pilot's ability to maintain control of the aircraft and to deal with strong gusts encountered in the unsteady airwake is reduced.

The demanding nature of ship-borne helicopter operations means that every ship/helicopter combination has its own specific Ship-Helicopter Operating Limits (SHOLs) which are derived from First of Class Flight Trials. Due to the expenses and inherent dangers associated with such trials much of the research concerning the ship-helicopter dynamic interface has focused on the development of high-fidelity flight simulation [12-16] to augment at-sea SHOL trials and mitigate their costs and risks.

Recent work at the University of Liverpool has demonstrated that realistic unsteady ship airwakes can be computed using time-accurate CFD and implemented in a full-motion flight simulator to enable a pilot to land a helicopter onto a ship in a high-fidelity simulation environment [15, 16]. The disturbances experienced by the pilot and the workload required to perform landings was shown to be representative of the at-sea environment. It is therefore possible to obtain a fully-simulated SHOL using these sophisticated tools and techniques. In addition, it is now also possible to use these techniques to investigate different ship geometries and to explore how favourable, or otherwise, their landing deck is to a helicopter.

Helicopter operations to non-aviation ships such as single-spot frigates are particularly susceptible to adverse airwake effects. Although attempts have been made to control the airflow over such ships [17, 18], little practical progress has been made. The long term objective of the work reported herein is to look beyond the ship-helicopter dynamic interface as defined by existing ship geometries by investigating how current ships can be modified and ships of the future can be designed so as to alleviate the effect of the airwake on pilot workload, easing the demands on the pilot and broadening operational envelopes. However, the use of piloted flight simulations to investigate the effect of design changes is likely to be a time-consuming and expensive process, particularly if numerous design iterations are required. The objective of the study being reported here is the development of a method that will allow the assessment and comparison of the airwakes of different ship geometries without the need for piloted simulation.

The method involves holding a simulated helicopter model fixed in space immersed in a CFD ship airwake and measuring the unsteady forces and moments at the model's centre of gravity. It is widely accepted that airwake induced disturbances in the aerodynamic loading and rotor response is a major cause of excessive pilot workload [9]. Therefore, it is proposed that these loading characteristics can be used as a measure of the severity of a ship's airwake and will enable the comparison of different ship geometries in terms of their potential pilot workload characteristics.

Figure 1: Sea-Hawk SH-60B helicopter

A simulation model of a Sea-Hawk (SH-60B) helicopter (Fig. 1) has been fixed in space at various points relative to the flight deck of a Simple Frigate Shape (SFS2) (Fig. 2). The model has then been subjected to a time-accurate SFS2 airwake, generated using CFD with a Detached-Eddy Simulation (DES) turbulence model, for a period of 30 seconds. The unsteady forces and moments imparted to the model as a result of the airwake have then been recorded and analysed in terms of

potential pilot workload. The unsteady aerodynamic loading at the various test points has been used to identify specific loading characteristics of an SH-60B helicopter in the wake of an SFS2 for two WOD conditions. The SFS2 airwake aerodynamics data has also been presented to identify the underlying causes of the loading characteristics encountered in the simulations.

Simple Frigate Shape 2 (SFS2)

The SFS2, shown in Fig. 2, is a generic frigate shape created under the auspices of The Technical Cooperation Program (TTCP) as a means of comparing the numerous CFD codes of researchers from the member states. The SFS2 has been chosen for this initial study because of its relatively simple geometry and flow features compared with more realistic frigate shapes such as the Royal Navy Type 23 Frigate. Future work will build on this study to investigate more realistic ship shapes. A further benefit of using the SFS2 is the availability of high quality wind-tunnel data from experiments provided by the National Research Council of Canada (NRC), which has been used to validate the CFD airwakes used in this study. Comprehensive comparisons between CFD and experimental data can be found in the study by Forrest and Owen [6].

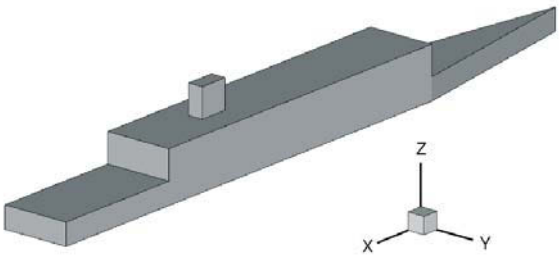

Figure 2: Simple Frigate Shape (SFS2)

Computational Fluid Dynamics (CFD)

The unsteady airwake data was generated using the commercial CFD code FLUENT, using Detached-Eddy Simulation (DES) to capture the large-scale turbulent structures. Using an unstructured mesh containing approximately 6 million cells, the computations were partitioned across 32 processors of the University of Liverpool's high performance computing cluster, taking about 60 hours to generate 30 seconds of full-scale airwake data. This airwake generation method has been extensively validated against model-scale and full-scale data [6, 15, 16], where it has been shown that the spatial and temporal characteristics of the airwake are well modelled.

Airwake data was interpolated onto a structured grid for export to the FLIGHTLAB simulation environment, utilising a spatial resolution of 1m and an update rate of 20 Hz.

Rotorcraft Model

A UH-60A rotorcraft simulation model has been re-configured to be representative of a Sea-Hawk (SH-60B) helicopter. The model was developed using FlightLab, an advanced multi-body dynamics modelling and simulation environment, which allows complete rotorcraft simulations to be constructed from a set of modular components (e.g. main/tail rotors, fuselage and empennage). In order for the ship airwake to affect the aerodynamic loading of the simulated rotorcraft model the airwake velocity components must be converted into forces and moments at the helicopter's centre of gravity. To do this the airwake velocity components are interpolated from a look-up table at a total of 24 Aerodynamic Computation Points (ACPs) distributed around the model as shown in Fig. 3 (the pictured helicopter is not representative of an SH-60B and is for illustration purposes only). This includes the fuselage, empennage, tail hub and five elements along each of the four main rotor blades.

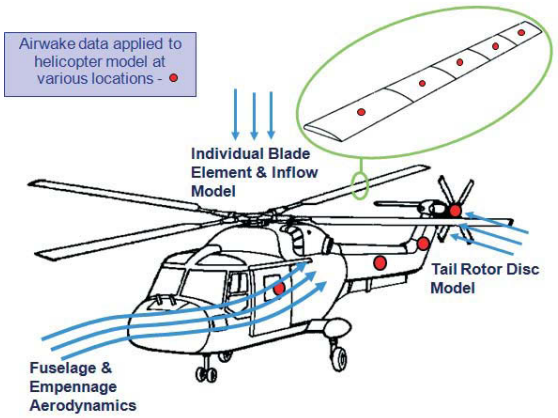

Figure 3: Location of 24 Aerodynamic Computation Points (ACPs)

The aircraft setup includes a dynamic inflow model and also accounts for the effect of rotor downwash. However, the coupling between the ship airwake and the aircraft model is 'one-way' in that the airwake affects the helicopter response but is not, in turn, influenced by the rotor downwash. The importance of fully coupled airwake/rotor-downwash simulations is not yet clear [19], however future work at the University of Liverpool plans to investigate this further.

Test Program and Data Acquisition

This study has employed the use of naval terminology, such that 'green' and 'red' refer to the starboard and port sides of the ship respectively. Therefore a G30 wind denotes a WOD angle of thirty degrees from the longitudinal centreline of the ship, originating from the right hand side when looking towards the bow. In the discussions to follow, velocity and turbulence data is normalised by free-stream velocity. Longitudinal, lateral and vertical spatial coordinates (x, y, z) are normalised by deck length (l), ship beam (b) and hangar height (h) respectively.
The helicopter model was trimmed with an airspeed of 40kts at a wind direction consistent with the airwake WOD angle. The trim was required to reduce the effect of the lift imbalance between the advancing and retreating blades; the resulting collective and cyclic pitch angles are shown below in Table 1. These values were retained throughout the simulations at each test point.

WOD azimuth	Collective pitch	Lateral cyclic	Longitudinal cyclic
Headwind	15.25°	-2.50°	2.36°
G30	15.16°	-1.64°	3.05°

Table 1: Collective and cyclic blade pitch angles

The aircraft was then placed, in turn, at 49 points relative to the SFS2 flight deck as shown in Fig. 4. The rotor hub vertical (*z*) position was maintained at a constant height of 6.1 m above the flight deck, which corresponds to the height of the top the hangar from the deck.

Once fixed at a particular test point, the model's translational and rotational degree of freedom states were disabled and the unsteady airwake (scaled to a WOD speed of 40 kts) was run for a period of thirty seconds; this procedure was performed for a headwind and Green 30° (G30) WOD azimuth.

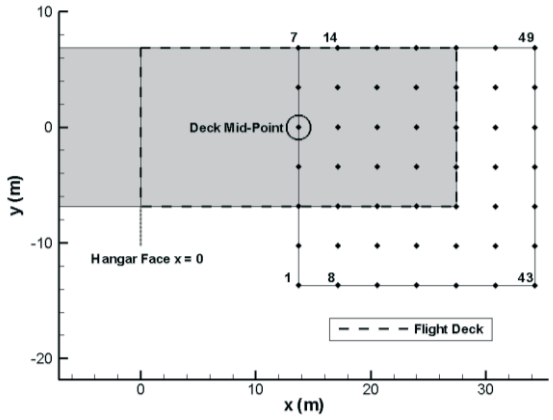

Figure 4: Locations of helicopter model centre of gravity in relation to the SFS2 flight deck

The thirty second time-histories of the unsteady forces and moments at the model's centre of gravity were recorded. This data has been time-averaged to enable comparisons of the mean aerodynamic loading characteristics between the test points and WOD conditions.

The simulated unsteady aerodynamic loading characteristics have been generated using the method adopted by Lee and Zan [10, 11] in their experimental investigations of the aerodynamic loading of a helicopter fuselage and rotor in a ship airwake. It is known that disturbances in the frequency range 0.2 – 2 Hz have the most significant impact on helicopter handling qualities and pilot workload [20]. Therefore, when performing statistical analysis of unsteady loading, using the root-mean-square (RMS) of the deviations from the mean is not the ideal way to quantify the impact of the airwake as it includes fluctuations at frequencies outside the bandwidth known to be responsible for airwake induced pilot workload. Instead, Power Spectral Density (PSD) plots have been derived from the force and moment time-histories and the square root of the integral between the limits 0.2 – 2 Hz (displayed graphically in Fig. 5) has been used as a measure of the RMS loading in this frequency bandwidth. This quantity will hereby be referred to as the RMS loading of the particular force or moment in question (e.g. RMS yawing moment). The RMS loading in each of the 6 degrees-of-freedom has been used to characterize unsteady aerodynamic loading of the SH-60B as a result of the SFS2 airwake.

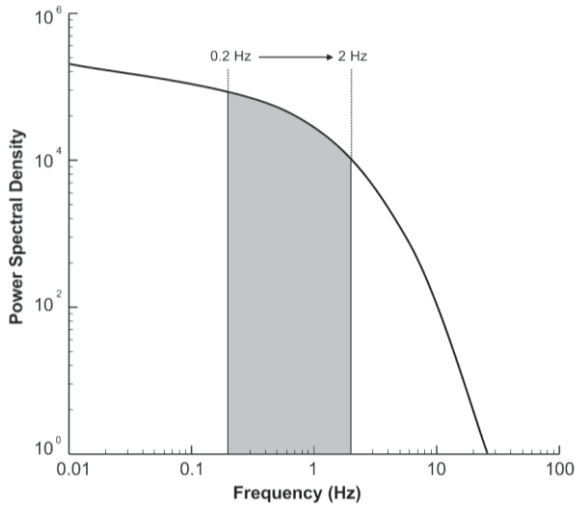

Figure 5: Closed loop pilot response frequency bandwidth

Standard Royal Navy Landing Technique

The unsteady aerodynamic loading data presented in this paper has been analysed in such a way that it relates to the standard Royal Navy landing approach technique (Fig. 6). A typical ship-helicopter landing operation comprises a series of Mission Task Elements (MTEs) as follows:

1) Approach and port-side hover
2) Lateral translation
3) Station keeping over the flight deck
4) Vertical descent to landing spot

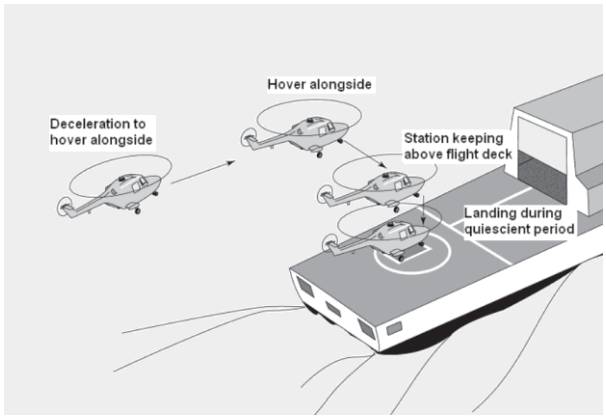

Figure 6: Final stages of the recovery of a Royal Navy helicopter to a single spot frigate

The operation begins with an approach alongside the flight deck to a stabilised hover to the port side of the ship. The pilot then executes a lateral translation across the deck to a stabilised hover over the landing spot. The pilot then maintains station over the spot until there is a quiescent period in the ship's deck motion, before finally executing a descent to the flight deck.

For the purposes of this study the landing spot is assumed to be on the centreline of the SFS2 at a longitudinal location halfway between the hangar face and the stern.

Results and Discussion

Thrust Characteristics – Headwind

The time histories of thrust at the headwind condition for points 1, 3 and 5 (identified in Fig. 4) are shown in Fig. 7. These points are all on a lateral line aligned with the landing spot which corresponds to the approximate path of the lateral translation MTE. Figure 7 indicates that as the aircraft model translates from the port-side to the centreline of the ship, moving from the freestream to a location fully immersed in the airwake, mean thrust decreases and the magnitude of thrust fluctuations increases.

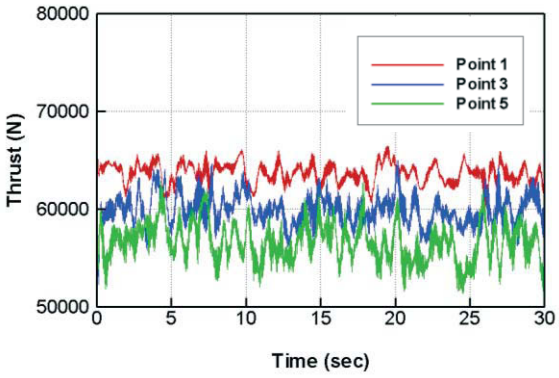

Figure 7: Time-histories of thrust in a headwind at points along the approximate path of the lateral translation MTE at x/l = 0.5

Figure 8 shows the time-averaged thrust coefficient (C_T) plotted against lateral deck position for various distances from the hangar face. At the longitudinal location *x/l* = 0.5, aligned with the landing spot, there is a reduction in thrust of approximately 11% as the aircraft moves laterally from the freestream to the ship centreline. This trend is consistent with the experimental study of rotor thrust in a ship's airwake by Zan [21].

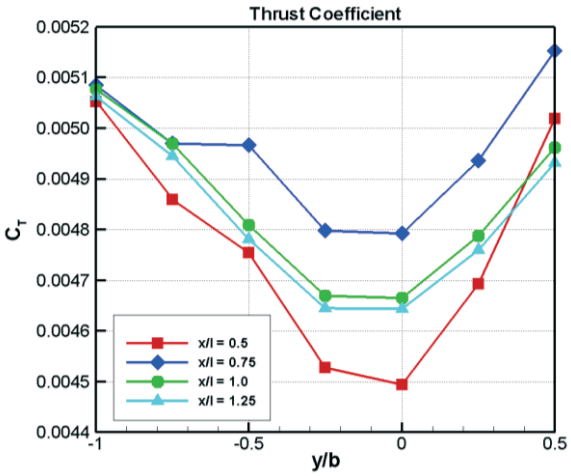

Figure 8: Time-averaged thrust coefficient in a headwind at various longitudinal locations

During a real landing manoeuvre, this loss of thrust over the flight deck during the lateral translation MTE would require the pilot to increase the collective pitch of the main rotor blades in order to maintain the altitude of the aircraft. This would reduce the available thrust control margin and adversely impact the pilot's ability to respond to fluctuations in lift caused by the unsteady airwake. Reduction of the thrust control margin is a common issue associated with headwind ship deck landings, especially for low WOD speeds [9].

The cause of this behaviour can be identified by studying the underlying aerodynamics of the SFS2 airwake. Figure 9 shows the time-averaged velocity streamlines over the centreline of the SFS2 flight deck for a headwind, coloured by the vertical velocity component. The airflow comes over the top of the hangar and reattaches to the flight deck approximately halfway along the deck, creating a significant downward component to the mean velocity of the airwake. As the helicopter translates over the flight deck a reduction in thrust is observed because the steep down drafts over the deck reduce the effective angle of attack of the main rotor blades and hence the amount of thrust force produced by the main rotor. This effect is also exacerbated by the reduction in longitudinal velocity experienced by the rotor disk as it passes into the recirculation region behind the hangar. Figure 10 shows contours of mean longitudinal velocity. When the helicopter model is over the deck, there will be a lower induced velocity to the main rotor blades therefore reducing the mean thrust produced.

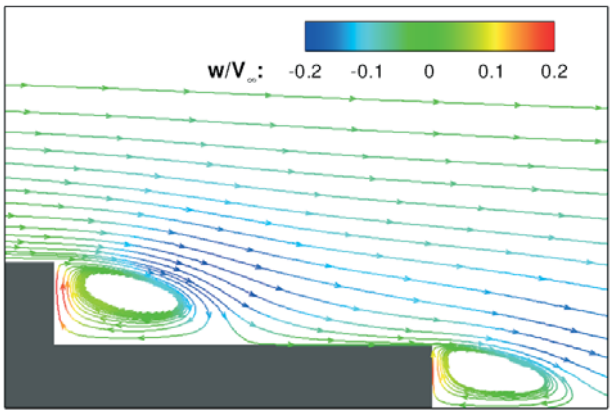

Figure 9: Mean velocity streamlines coloured by vertical velocity in the plane y/b = 0 for a headwind

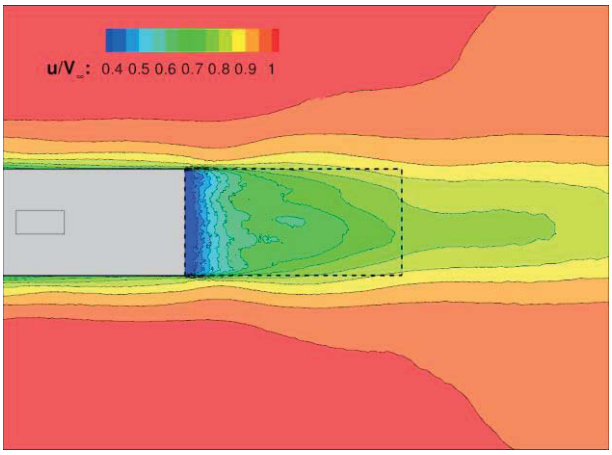

Figure 10: Contours of longitudinal mean velocity in the plane z/h = 1.0 for a headwind

Figure 8 shows that other longitudinal positions also exhibit the trend of decreasing mean thrust over the flight deck, although the loss of thrust is not as severe as the distance from the hangar increases. At a longitudinal position of $x/l = 0.75$, the loss of thrust is reduced as the flow is aligned more with the horizontal after reattachment (Fig. 9). At locations towards the rear of the flight deck the flow is again deflected downwards due to separation from the stern, causing a corresponding reduction in thrust.

The thrust distribution across the deck, shown in Fig. 8, is asymmetric which is again consistent with Zan's findings [21]. When the model is on the port side of the ship's centreline the advancing blades of the counter-clockwise rotor are in the lower velocity wake region and the retreating blades are in the higher velocity freestream region (Fig. 10). On the starboard side of the centreline the opposite is true and the advancing blades are

in the higher velocity region. As a result, both the advancing and retreating blades are producing less lift at y/b = -0.5 than at y/b = 0.5, due to the former operating in a region of lower velocity and the latter exposed to freestream velocity. The net effect is that thrust over the starboard deck edge is approximately 4% higher than the port edge.

The time-histories in Fig. 7 also show significant fluctuations in thrust, with variations in amplitude seen between the three points. To examine this further, spectral analysis has been performed, with the resulting PSD plots shown in Fig. 11. At each of the points there is significant energy in fluctuations within the pilot closed-loop response frequency bandwidth of 0.2 – 2 Hz. These disturbances in the thrust produced by the helicopter will impact on pilot workload as the pilot responds through their collective control to maintain a stable aircraft altitude. This control axis is particularly critical due to the aircraft's close proximity to the deck. The plots also show significant energy in disturbances at higher frequencies. These high frequency loading fluctuations, caused by the rotor harmonics, are an inherent effect of the cyclical nature of rotorcraft thrust generation. As these peaks occur at frequencies above 10 Hz they can be safely ignored in terms of pilot workload analysis, manifesting themselves as vibrations rather than disturbances which must be counteracted though pilot control inputs.

As this study is primarily concerned with the loading fluctuations in the closed loop pilot response frequency range, the RMS thrust over this reduced bandwidth has been calculated as described earlier. Figure 12 shows RMS thrust plotted against lateral deck position for various longitudinal distances from the hangar face, which includes the three points in Figs 7 and 11. Figure 12 shows that as the aircraft translates from the port side of the deck into the turbulent airwake over the deck, the RMS thrust increases. This is to be expected, due to the rotor being fully immersed in high levels of turbulence over the landing spot. Thus, as the pilot executes the lateral translation MTE not only will the thrust control margin available to them be reduced but the workload required to maintain a stable hover altitude will increase as result of the greater unsteadiness in the RMS thrust. The combination of these two factors is especially problematic as a reduced control margin will impact on the pilot's ability to respond to fluctuations in this axis.

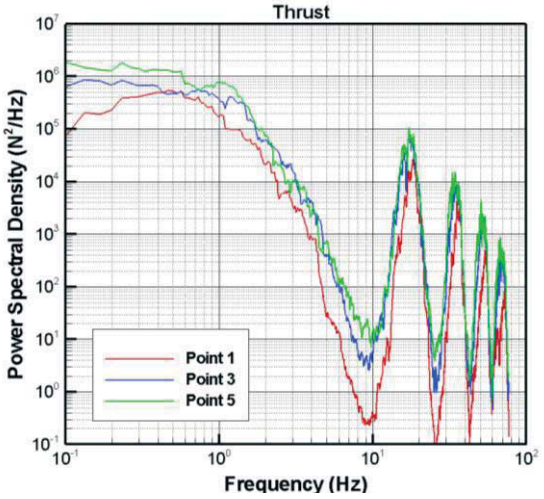

Figure 11: Power Spectral Density of thrust for the headwind condition at three locations relative to the flight deck

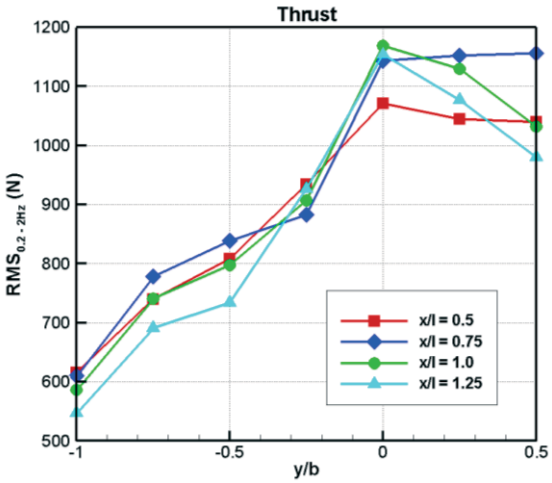

Figure 12: RMS thrust for various helicopter positions

Figure 12 also shows that RMS loading is asymmetric across the deck and is higher on the starboard side of the ship centreline. As the turbulence is reasonably symmetrical across the deck for a headwind, it is postulated that this asymmetry is a function of the rotational direction of the main rotor and the orientation of the SH-60B tail rotor. A definitive explanation of this phenomenon will require further investigation possibly through the use of simplified rotorcraft models.

Effect of WOD azimuth

In this section the RMS forces and moments for the headwind and G30 WOD conditions have been analysed to identify their specific loading characteristics. Figure 13 shows contour plots of RMS roll moment for the two wind conditions. Greater levels of RMS roll moment are evident in the G30 case, especially towards the port side of the deck. This is because of the greater unsteadiness of the airwake in these regions which can be seen in the longitudinal turbulence intensity contours shown in Fig. 14.

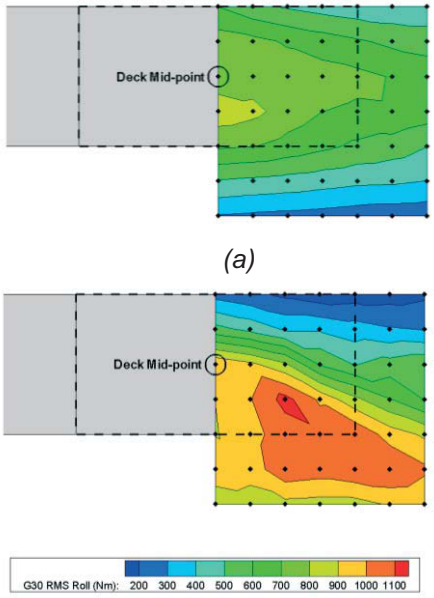

(a)

(b)

Figure 13: Contours of RMS roll moment for headwind (a) and G30 (b) WOD angle

The high levels of turbulence over the flight deck in the G30 case are caused primarily by shear layer separation from the top edge and windward vertical edge of the hangar [6] which leads to the increased RMS roll moments compared with the headwind case. The increase in roll unsteadiness in the closed pilot loop response bandwidth will increase the pilot workload required to maintain aircraft stability throughout the station keeping MTE over the flight deck. This was seen in the piloted flight simulation study by Forrest *et al.* [16] involving a Lynx helicopter and SFS2 airwakes, where G30 WOD conditions resulted in greater pilot workload when compared with the headwind case.

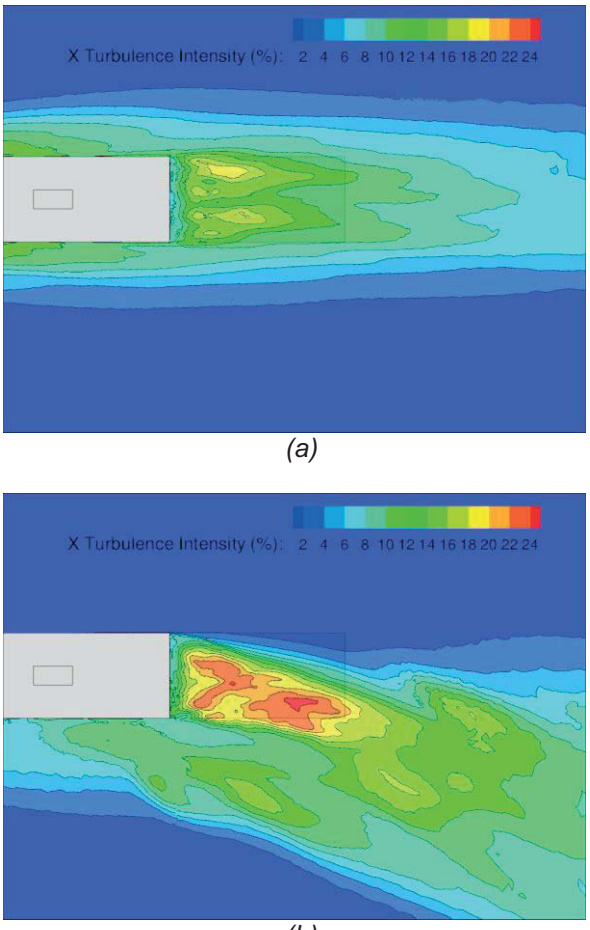

(a)

(b)

Figure 14: Contours of longitudinal turbulence intensity for headwind (a) and G30 (b) in the plane z/h = 1.0

The greater roll moment unsteadiness for a G30 wind is also evident when the aircraft is positioned to the port side of the ship. The higher levels of turbulence in this region, caused by the shedding of vortical structures from the windward edge of the superstructure, are the source of the greater unsteady loading. This means that pilot workload during the port-side hover and lateral translation will also be greater for the G30 case. The RMS loading in the headwind case is low at the port-side approach and increases as the helicopter translates into the turbulent wake over the deck. The G30 case on the other hand has an equally significant RMS roll moment at the location of the portside hover and along the path of the lateral translation as over the flight deck. This will cause the pilot to work hard to control the aircraft for a considerably longer time period than for a headwind landing. Therefore, it is suggested that future work should investigate ways of mitigating

the effects of port-side airwake turbulence through geometrical modifications to reduce pilot workload during the port-side hover and lateral translation MTEs.

Figure 13 also shows that on the starboard side of the deck the RMS roll loading is greater for the headwind compared with the G30 WOD angle. This because in the G30 case most of the main rotor and the tail rotor have moved out of the turbulent airwake into the lower turbulence, higher mean velocity, freestream region. Figure 13 shows how the RMS roll loading, in the G30 case, falls sharply after the helicopter passes the centreline of the ship towards the starboard side. In comparison, the RMS loading in the headwind case remains relatively constant across the deck due to the smaller spatial gradients of turbulence across the deck. As with the RMS thrust for the headwind case discussed earlier the RMS roll moment is asymmetric across the deck but this time with higher values on the port side. Again it is suggested that this is an effect of the rotational direction of the main rotor and the configuration of the inclined SH-60B tail rotor which will significantly affect pitch, roll and yaw characteristics.

Effect of Hover Position

Figure 15 shows a comparison of RMS loading for two helicopter locations, over the sea on the portside and over the landing spot. In the headwind case, RMS loading is greater over the spot in every degree of freedom. This is because in this location, the helicopter model is fully immersed in the highly turbulent airwake. The unsteadiness in the airflow causes fluctuations in the aerodynamic loading and rotor response of the helicopter in the closed loop pilot response frequency range. When the model is positioned at the port side hover, the lower turbulence levels in the airflow have led to lower RMS loadings than over the spot.

Therefore, during a deck landing operation in this WOD condition, the pilot workload required to maintain a stable aircraft attitude, heading and altitude will increase as the helicopter translates over the deck to the position of the station keeping MTE. This was observed is piloted flight simulation trials conducted by Forrest *et al.* [16], where pilot comments consistently reported the highest workload to be when the helicopter was over the deck.

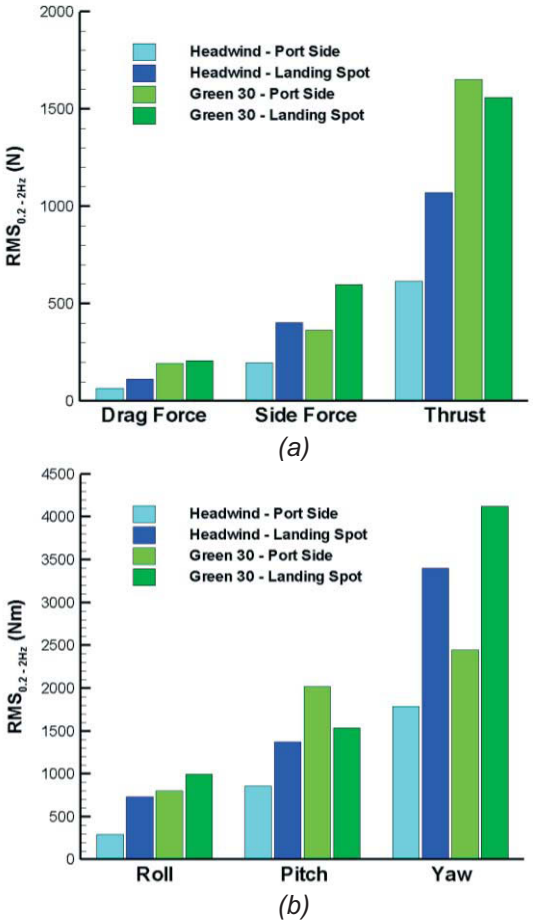

Figure 15: RMS loading comparison of forces (a) and moments (b) for the port side and landing spot hover locations

In the G30 case, such a clear difference in the RMS loading between the two WOD conditions does not exist. Figures 15a and 15b show that RMS loading in the side force and yaw axes is greater over the landing spot. This is because of a large unsteadiness in the lateral velocity component of the airwake in this region. This unsteadiness is caused by the flapping shear layer created as the flow separates from the windward, vertical edge of the hangar [6]. Figure 16 shows that the greatest lateral turbulence intensity is concentrated over the flight deck. The lateral unsteadiness in the airflow leads to fluctuations in the aerodynamic loading of the fuselage and tail rotor, resulting in an RMS loading over the spot which is 39% and 40% greater than over the port side for side force and yaw respectively.

The headwind case also has a greater RMS side force and yawing moment over the spot compared with the port side hover. As with the

G30 case, the greater unsteadiness of the lateral velocity component of the airflow interacting with the fuselage and tail rotor in this region has resulted in the larger RMS loadings when the model is over the spot. This suggests a link between unsteady side force and yawing moment and that these quantities are especially sensitive to the lateral turbulence of the airwake.

The ability to identify specific loading characteristics and their underlying aerodynamic causes is a key advantage of using the method employed in this study. It will enable the identification of airwake features that are particularly detrimental to helicopter handling qualities and exactly how these flow features manifest themselves in terms of unsteady aerodynamic loading and rotor response. Thus, ship design changes or modifications can be implemented to specifically target such features and mitigate their effects on pilot workload. For example, if a particular ship's airwake is known to cause large disturbances in the yaw axis, a clear correlation like the one drawn above would lead to ship modifications targeting the reduction of airwake lateral turbulence. The method employed in this study could then be used to assess the effect of such modifications on the unsteady yaw characteristics of a helicopter in the airwake.

Figure 15a shows that, in the G30 case, the unsteady thrust characteristic differs from side force and yaw in that RMS thrust is slightly greater for the port side hover position than for over the landing spot. To identify the reasons behind this observation it is necessary to look at the vertical turbulence intensity in the airwake shown in Fig. 17. Although the longitudinal and lateral turbulence is greater in the region over the spot, Fig. 17 shows that the vertical airwake turbulence is greatest over the port edge of the deck. There is also a region of relatively high vertical turbulence intensity over the sea approximately one rotor diameter to the port side of the deck. The large unsteadiness in the vertical velocity component in this region is caused by vortical structures emanating from the top windward edge of the superstructure and funnel [6].

The thrust response of the helicopter is sensitive to turbulence in the vertical direction because as the vertical velocity component of the airwake fluctuates, so too will the effective angle of attack of the induced airflow to the main rotor blades and therefore the magnitude of the thrust force produced [22]. When the helicopter is in the port side hover position, both the advancing and retreating blades are interacting with airflow containing a large vertical unsteadiness. The influence of the unsteady vertical velocity component is the principal reason behind the greater RMS thrust observed for the port side hover location.

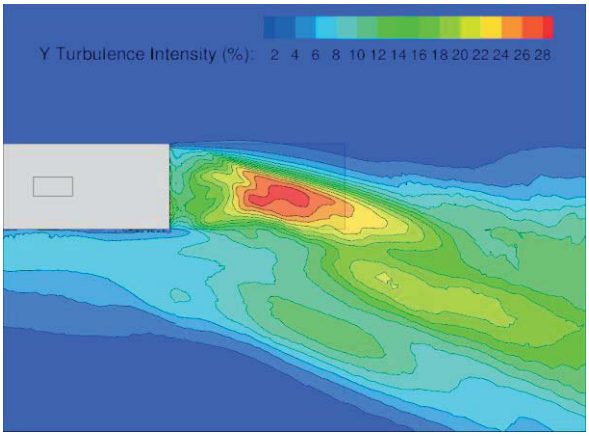

Figure 16: Contours of lateral turbulence intensity in the plane z/h = 1.0 for G30 WOD condition

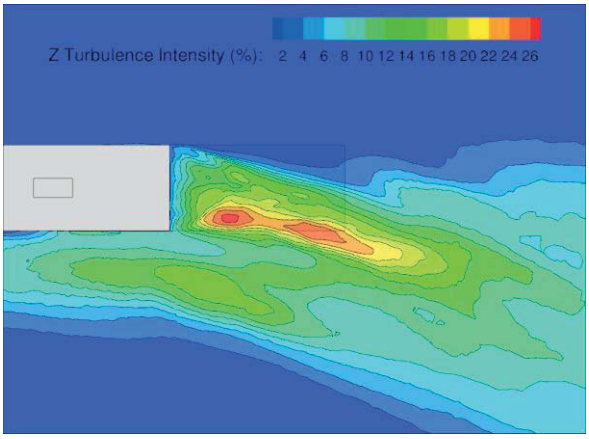

Figure 17: Contours of vertical turbulence intensity in the plane z/h = 1.0 for G30 WOD condition

Figure 15a shows that the unsteady thrust characteristic is different for the G30 WOD condition and the headwind case discussed earlier. RMS thrust is greater in the G30 case because of the greater turbulence intensities in all three directions. However, whereas in the headwind case unsteadiness in the thrust increases as the helicopter translates over the deck, in the G30 case RMS is equally significant over the port side hover. Larger amplitude loading fluctuations in the closed loop pilot response frequency bandwidth seen in the G30 case will make it more difficult for the pilot to respond to disturbances and maintain aircraft stability. Therefore, the greater RMS thrust over the spot in the G30 case will enforce a greater

pilot workload during both the station keeping and port side hover MTEs. This will make a landing task much more demanding as the pilot has to work hard to maintain a stable altitude for a longer period of time.

Figure 15b also shows that in the G30 case the RMS pitch moment is greater at the port side hover compared with over the spot. At this location the advancing blades of the rotor are passing through the region of high vertical turbulence intensity over the port deck edge (Fig. 17). Due to the 90° phase shift, these fluctuations in the vertical velocity component will manifest themselves as disturbances in the pitch of the aircraft. This, in turn, has resulted in the greater RMS pitching moment for the port side hover shown in Fig. 15b.

RMS yawing moment in a G30 wind

Figure 18 shows PSD plots of yawing moment for three different lateral locations along *x/l* = 0.5. All three points show significant energy in the closed loop pilot response frequency range, with the corresponding RMS yawing moments over this bandwidth shown in the legend. The greatest RMS yaw moment is observed when the model is at point 4; this point has been chosen for analysis because in this position the main and tail rotor are fully immersed in the highly unsteady region of the airwake caused by the flapping shear layer created by the flow separation from the windward vertical edge of the hangar [6].

Figure 19 shows the areas swept by the main rotor blades of the model SH-60B at the three locations, superimposed onto a contour plot of lateral turbulence intensity for a G30 wind. The airflow interacting with the side of the fuselage and tail rotor blades at point 4 is highly turbulent and leads to a large unsteadiness in the yaw moment in the closed loop pilot response frequency bandwidth.

Figure 18 also shows that Point 1 has a large RMS yaw loading at G30 due to the turbulence over the port side, caused by the large scale flow structures emanating from the windward side of the superstructure [6]. When the helicopter model is at Point 7, over the starboard edge of the deck, most of the fuselage, main rotor and tail rotor are no longer interacting with the highly turbulent airwake and are instead immersed in the lower turbulence freestream region. This has resulted in a significantly lower RMS yawing moment at this point because of the removal of the majority of the disturbances in this axis as a result of the airwake.

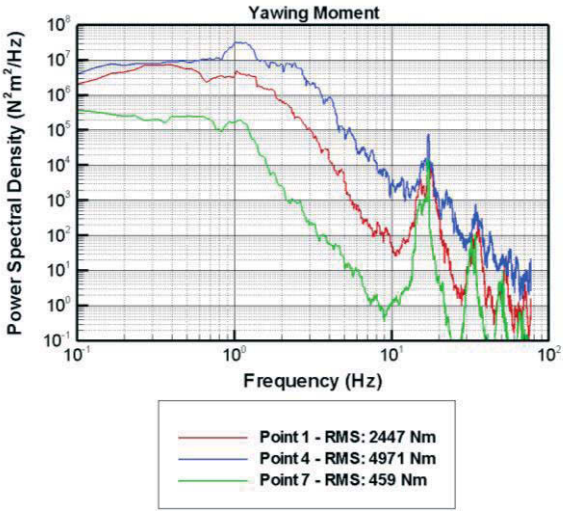

Figure 18: Power Spectral Density of yawing moment for G30 WOD angle at three points along x/l = 0.5

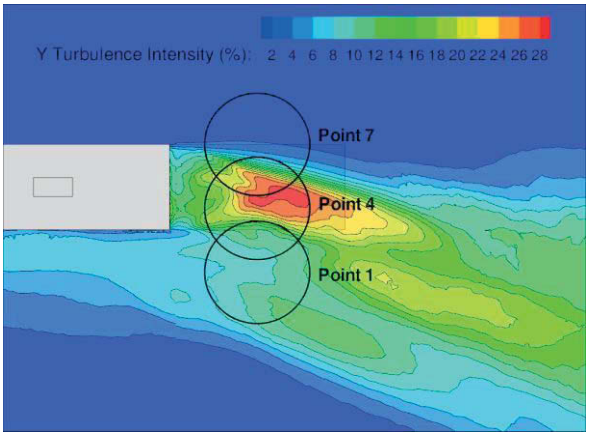

Figure 19: Contours of longitudinal turbulence intensity in the plane z/h = 1.0 and the areas swept by main rotor blades

As the pilot translates the helicopter over the deck a significant portion of their workload will be directed towards responding to unsteady yaw disturbances caused by the unsteady airwake. In the G30 case, the RMS yaw moment is also greatest over the flight deck where the pilot is under most pressure to maintain stable attitude and heading before any attempted descent to the landing spot. Therefore it is recommended that future investigations into ship superstructure modifications should focus on reducing the effects of shear layer turbulence. There are several different possible methodologies that may achieve this, including the deflection of the shear layer

using various configurations of inclined screens or through the 'breaking up' of airwake turbulence into higher frequency disturbances that are outside the closed loop pilot response frequency range of 0.2 – 2Hz.

Conclusions

The aerodynamic loading of a model rotorcraft based on an SH-60B helicopter, fixed in space at various points relative to the flight deck of an SFS2, has been simulated for a headwind and G30 WOD azimuth.

Time-averaged and unsteady loading characteristics caused by the airwake have been identified. The loading characteristics have been analysed and compared for various helicopter locations at the two WOD conditions. The underlying aerodynamics of the airflow over the SFS2 have also been analysed and the principal reasons behind the loading characteristics encountered in the simulations have been identified. Correlations have been found between particular airwake flow features and unsteady loading characteristics.

It is concluded that the method employed in this study is a suitable technique for the investigation of the effect of ship geometry modifications on helicopter handling qualities.

Future work will use this method to investigate the effect of ship geometry on aerodynamic loading of a helicopter in the airwake. This technique will be used to assess the effect of modifications to the SFS2 geometry in the attempt to mitigate the impact of the unsteady airwake on pilot workload. This work will also be extended to more realistic ship shapes such as the Royal Navy Type 23 Frigate and Type 45 Destroyer.

Acknowledgements

The authors are grateful to EPRSC for their ongoing financial support. ANSYS Inc. have also provided valuable assistance. The authors would like to thank Phillip Perfect from the Flight Science and Technology research group for his guidance and expertise.

References

[1]Cheney, B.T., Zan, S.J., CFD Code Validation Data and Flow Topology for The Technical Co-operation Program AER-TP2 Simple Frigate Shape, *National Research Council of Canada*, Report LTR-LA-294, 1999.

[2]Zan, S.J., Surface Flow Topology for a Simple Frigate Shape, *Canadian Aeronautics and Space Journal,* Vol. 47 (1), 2001, pp. 33-43.

[3]Johns, K.M., Healey, J.Val., The Airwake of a DD-963 Class Destroyer, *Naval Engineer's Journal,* Vol. 101**,** No.3, 1989, pp 36-42.

[4]Healey, J.Val., Establishing a Database for Flight in the Wakes of Structures, *Journal of Aircraft*, Vol. 29, No. 4, 1992, pp. 559-564.

[5]Rhoades, M.M., Healey, J.Val., Flight deck Aerodynamics of a Nonaviation ship, *Journal of Aircraft*, Vol. 29, No. 4, 1992, pp. 619-626.

[6]Forrest, J.S., Owen, I., Investigation of Ship Airwakes using Detached-Eddy Simulation, *Computers and Fluids*, Accepted for publication, 2009.

[7]Polsky, S.A. and Bruner, C.W., Time-accurate computational simulations of an LHA ship airwake, AIAA Paper 2000-4126, *18th Applied Aerodynamics Conference and Exhibit*, Denver, CO, 14-17 August, 2000.

[8]Polsky, S.A. A Computational Study of Unsteady Ship Airwake, AIAA Paper 2000-4126, *40th Applied Aerospace Sciences Meeting and Exhibit*, Reno, NV, 14-17 January, 2002.

[9]Zan, S.J., On aerodynamic modelling and simulation of the dynamic interface, *Proceedings of the Institution of Mechanical Engineers, Part G: Aerospace Engineering*, 2005, 219, pp 393-410.

[10]Lee, R.G., Zan, S.J., Unsteady aerodynamic loading on a helicopter fuselage in a ship airwake, *Journal of the American Helicopter Society*, Vol. 47, No.2, April 2004.

[11]Lee, R.G., Zan, S.J., Wind tunnel testing of a helicopter fuselage and rotor in a ship airwake, 29th *European Rotorcraft Forum*, Freidrichstrafen, Germany, September, 2003.

[12]Roscoe, M. F., Thompson, J. H., JSHIP's Dynamic Interface Modeling and Simulation System: A Simulation of the UH-60A Helicopter/LHA Shipboard Environment Task, *59th Annual Forum*, Phoenix, AZ, 6-8 May, 2003.

[13]Hodge, S.J., Padfield, G.D., and Southworth, M.R., Helicopter-ship dynamic interface simulation: Fidelity at low-cost, *Cutting Costs in Flight Simulation - Balancing Quality and Capability*, RAeS Conference, London, UK, 2006.

[14]Hodge, S.J., Zan, S.J., Roper, D. M., Padfield, G.D., Owen, I., Time-Accurate Ship Airwake and Unsteady Aerodynamic Loads Modeling for Maritime Helicopter Simulation, *Journal of the American Helicopter Society*, Vol. 54, No.2, April 2009.

[15]Forrest, J.S., Hodge, S.J., Owen, I., and Padfield, G.D., Towards fully simulated ship-helicopter operating limits: The importance of ship airwake fidelity, *American Helicopter Society 64th Annual Forum*, Montréal, Canada, 29 April – 1 May, 2008.

[16]Forrest, J.S., Hodge, S.J., Owen, I., and Padfield, G.D., An investigation of ship airwake phenomena using time-accurate CFD and piloted helicopter flight simulation, *34th European Rotorcraft Forum*, Liverpool, UK, September 16-19, 2008.

[17]Findlay, D.B., Ghee, T., Experimental Investigation of Ship Airwake Flow Control for a US Navy Flight II-A Class Destroyer (DDG), *3rd AIAA Flow Control Conference,* San Francisco, CA, June 5-6, 2006.

[18]Greenwell, D.I., Barrett, D.V., Control of ship air wakes using inclined screens, *32nd European Rotorcraft Forum*, September 12-14, Maastricht, Netherlands, 2006

[19]Bridges, D.O., Horn, J.F., Alpman, E., and Long, L.N., Coupled Flight Dynamics and CFD analysis of pilot workload in ship airwakes, *AIAA Atmospheric Flight Mechanics Conference and Exhibit*, Hilton Head, SC, 20 – 23 August, 2007, Vol. 1, pp. 471 - 489

[20]McRuer, D.T., Interdisciplinary Interactions and Dynamic Systems Integration, *International Journal of Control,* Vol.59 (1), 1994, pp. 3-12.

[21]Zan, S.J., Experimental Determination of Rotor Thrust in a Ship Airwake, *Journal of the American Helicopter Society*, Vol. 47, No. 2, April 2002, pp. 100-108.

[22]Padfield, G.D. *Helicopter Flight Dynamics,* Blackwell, 2007.